PAPER • OPEN ACCESS

A study on casting of structural mesh-like metal parts

To cite this article: D Vlagkoulis *et al* 2021 *IOP Conf. Ser.: Mater. Sci. Eng.* **1037** 012017

A study on casting of structural mesh-like metal parts

D Vlagkoulis[1], A Vasileiou[2] and G-C Vosniakos[1*]

[1]National Technical University of Athens, School of Mechanical Engineering, Manufacturing Technology Section, Heroon Polytehniou 9, 15780 Athens, Greece
[2]The University of Manchester, Department of Mechanical, Aerospace and Civil Engineering, Manchester M1 3BU, United Kingdom

[*]Corresponding author's e-mail: vosniak@central.ntua.gr

Abstract. Mesh-like parts are employed in order to reduce weight of mechanical structures. This study focused on cylindrical shaped mesh-like spacers. First, the mesh shape was parametrically defined and mechanical strength and strain under specific combination of axial and shear loads were determined by numerical simulation. Manufacture of the best design was then investigated focusing on investment casting under both gravity and vacuum modes with a simple, yet uncommon, top feeding system. The best combination of casting mode and parameter values was determined by numerical simulation on commercially available dedicated software, considering solidification time and lack of defects as primary quality indices accompanied by an investigation of residual stress and deformation fields. To implement simulation-based decisions the part was investment-cast employing 3D printed dies for constructing the wax models.

1. Introduction

Recently, mesh-like components are increasingly used as light-weight replacements of full body parts in structural applications [1]. This trend has been particularly enhanced by Additive Manufacturing (AM) technologies having established themselves firmly due to their allowing for design freedom. In fact, a large stream of research is directed towards topological optimization of parts in view of 3D printing [2]; optimization may refer to the external shape or profile of the part, i.e. macro-scale [3], which is also the focus of this paper. In addition, optimization may also refer to part density, which is achieved by applying lattice structures at meso-scale [4], typically striving to achieve graded mechanical properties matching the expected loads [5]. Mesh-like structures at macro scale have been proposed for building machine frames [6], whereas truss-like structures, best known for a long time in connection to large structures such as bridges, have also been studied and optimized [7].

Mesh-like structures are conveniently manufactured by casting methods [8]. In order to save time and cost, before building molds to try out feeding architectures and casting parameters, it is desirable to evaluate them by simulation [9]. Due to the complexity of the casting process, involving multiphase flows, heat transfer and stress–strain fields coupled to temperatures in the presence of phase changes and microstructure formation, special software platforms are necessary as opposed to general purpose numerical simulation environments [10]. Such platforms have been reportedly exploited to assess casting quality by determining mold filling completeness, rate of solidification and solidification time, porosity and emergence of other defects, residual stresses, deformation including warpage, hot cracking sensitivity etc. [11], In addition, such simulations have been leveraged to produce data for establishing corresponding machine learning models [12].

This paper presents a case study of cylindrical structural mesh-like metal spacers. The aim is to advocate a work flow regarding improved design and manufacturing practices, starting with parametrically defined shapes, as presented in Section 2, proceeding with examining alternative casting deployment, as presented in Section 3, and ending up with prototype manufacture, as explained in Section 4. Conclusions of this study are outlined in Section 5 with a generalization flair.

2. Parametric part design study

The part that was studied was a cylindrical spacer of length 100 mm and diameter (D) of 10, 20 or 30 mm. The cylindrically shaped lattice is formed by a number of vertical rods of the same diameter (d) of 2,3,4 or 6 mm resulting in an angular spacing between rods (α) and a number of horizontal struts of circular cross section (diameter t of 1, 2 or 3 mm) forming circular patterns on horizontal equidistant planes (spaced at h), see figure 1(a). Parameters α, h and L have fixed values. The 24 alternative dimension combinations studied are shown in Table 1.

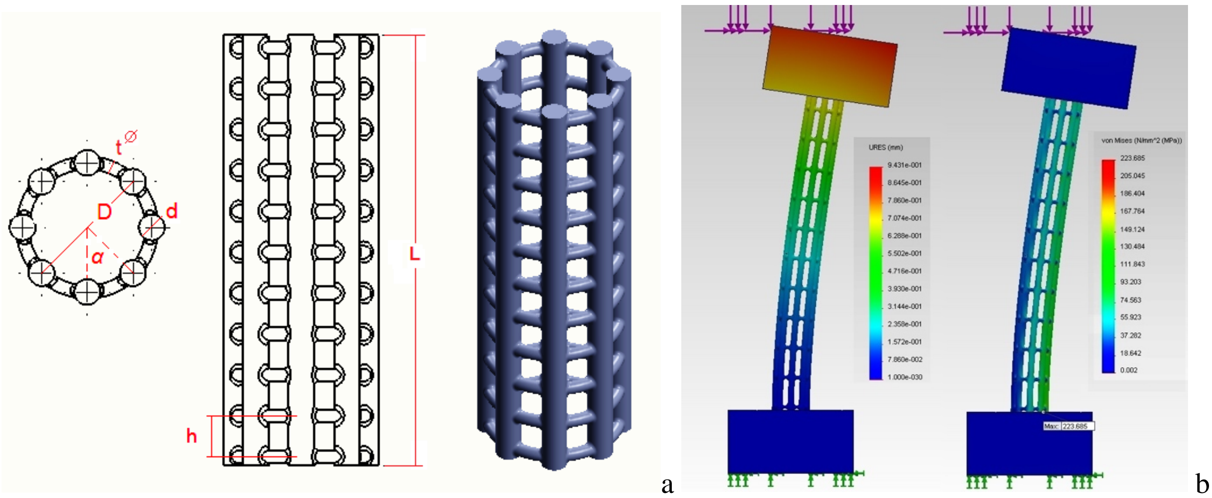

Figure 1. The spacer part (a) design involving 3 variable dimensions (D, d, t) and L=100mm, h=9mm $\alpha=45^{o}$ (b) static loading simulation example (displacement)

Table 1. Specimen specifications and simulation results.

specimen ID	1	2	3	4	5	6	7	8	9	10	11	12
D (mm)	10	10	10	10	10	10	20	20	20	20	20	20
d (mm)	2	2	2	3	3	3	2	2	2	4	4	4
t (mm)	1	2	3	1	2	3	1	2	3	1	2	3
Mass (gr)	7.3	8.7	11.6	15.7	16.4	17.9	8.1	11.6	18.2	28.1	30.5	34.6
Max stress (MPa)	224	184	193	77	98	93	221	203	148	101	52	40
Max displacement (mm)	-	-	-	0.40	0.38	0.36	-	-	0.24	0.14	0.08	0.07

specimen ID	13	14	15	16	17	18	19	20	21	22	23	24
D (mm)	20	20	20	30	30	30	30	30	30	30	30	30
d (mm)	6	6	6	2	2	2	4	4	4	6	6	6
t (mm)	1	2	3	1	2	3	1	2	3	1	2	3
Mass (gr)	61.7	63.0	65.1	8.8	14.6	24.8	28.9	33.4	41.2	62.5	65.9	71.7
Max stress (MPa)	30	24	19	268	182	122	112	50	39	51	28	18
Max displacement (mm)	0.04	0.03	0.03	-	-	0.15	0.22	0.07	0.04	0.06	0.03	0.02

The loads which the part needs to withstand are an axial force of 30 N and a shear force of 1500 N, applied at one end of the part, see figure 1(b). Both ends of the part are fixed on corresponding horizontal parallel plates which are considered rigid. These conditions are imposed by the machine environment in which the spacers are to function.

The spacer's material is aluminum alloy A356 T61 with minimum tensile strength 241 MPa and minimum yield strength 179 MPa, liquidus temperature: 616°C and solidus temperature: 556°C.

Solidworks Simulation™ was used in order to calculate maximum stress and, if that was lower than yield stress, maximum displacement of the spacer under static loading, see figure 1(b). The results are shown in Table 1.

In order to determine the best case, a suitable evaluation function was defined as follows:

$$\textit{Evaluation function} = \textit{mass (gr)} \; X \; \textit{maximum displacement (\%)} \; X \; \textit{maximum stress (\%)} \quad (1)$$

where *maximum displacement (%)* is the maximum displacement observed in the simulation divided by the maximum allowable displacement, which in this case was taken as 0.4 mm. Similarly, *maximum stress (%)* is the maximum stress observed in the simulation divided by yield strength of the material. Seven cases with max stress exceeding yield stress were crossed out. Note that the mass of the spacer is determined from its 3D model. The evaluation function value is plotted for all 17 valid specimens in figure 2(a). It becomes minimum for specimen No 24 followed by specimen No 15. In fact, for approximately the same mass widely varying stress and displacement corresponding to different specimen may be observed in figure 2(b). This is due to the different mass distribution corresponding to different dimensions of the respective specimen, see also Table 1.

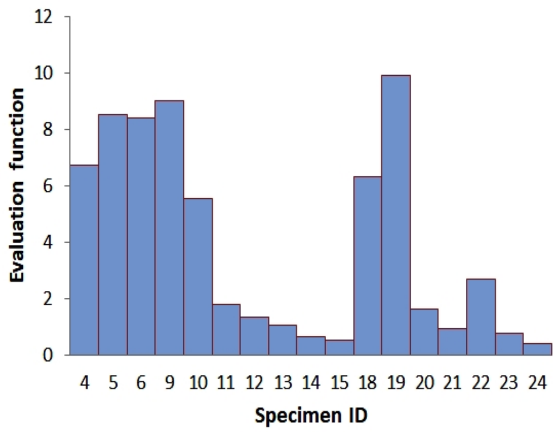

a

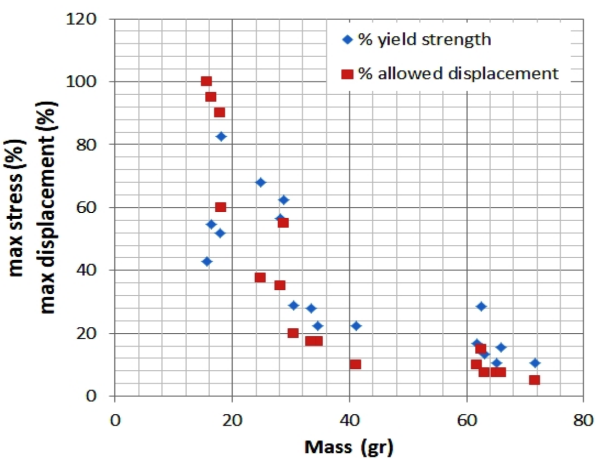

b

Figure 2. Part design simulation results (a) Evaluation function value per specimen (b) Normalised maximum stress and maximum displacement versus specimen mass for all 17 specimens

3. Casting method investigation

Gravity casting and vacuum assisted casting were the two methods studied by simulation in order to manufacture specimen No 24, which happens to be the largest one in the range examined. ProCast™ was used for this purpose, which supports filling as well as cooling for both thermal and mechanical domain. A direct top feeding system was designed, involving a top and bottom cylindrical plate of diameter 40 mm, at both ends of the spacer part. This is quite different from commonly applied solutions involving a sprue, runners and risers. In fact, the two plates act as risers in their own right, but feeding performance needed investigation anyway.

Mass inflow was approximately calculated using Bernoulli's equation for two different points of the conical sprue, i.e. one on the melt surface (A) and one on the inlet cross-section (B):

$$\dot{m} = \dot{Q}\,\gamma = \pi \frac{d^2}{4} \sqrt{\frac{2(p_A - p_B)}{\gamma} g + 2\,g\,|z_A - z_B|}\,\gamma \tag{2}$$

where z: z-coordinate, p: pressure at the respective points, γ: fluid density, d: sprue inlet diameter. For example, mass inflow was calculated at 1.14 Kg/s for gravity casting.

The main casting process parameters, i.e. melt temperature and mold initial temperature, were also investigated using two values for each one of them (650-700°C and 250-400°C respectively).

Note that the heat transfer coefficient which is needed in casting simulation setup [13] was available in the simulation platform's library referring to a standard aluminium-plaster interface.

3.1. Filling

Irrespective of the particular casting parameter values used filling of the mold in both gravity and vacuum cases was fully completed. Characteristic snapshots of the process are shown in figure 3. Filling time was 0.5 sec and 0.09 sec for gravity and vacuum casting respectively, see figure 3(a), whilst maximum velocity of the melt does not affect structural integrity of the mold, see figure 3(b).

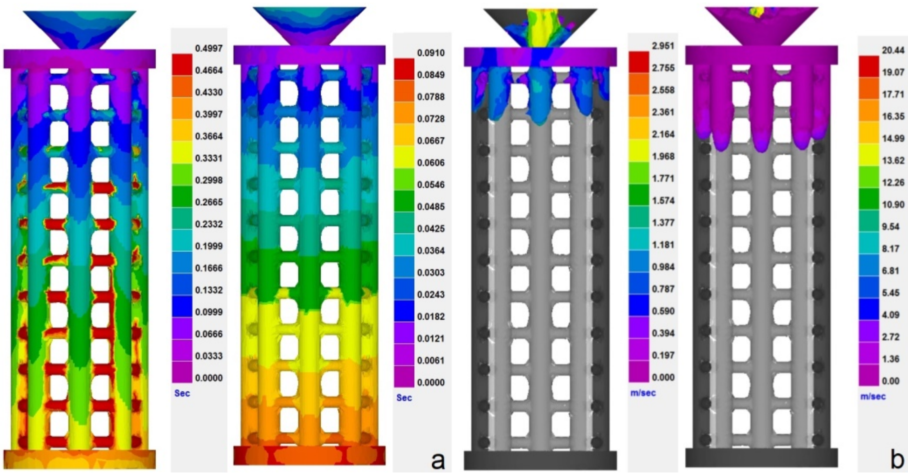

Figure 3. Mold filling (a) filling time (b) characteristic filling velocities (left: gravity, right: vacuum)

3.2. Solidification

Solidification study pertains to determining total solidification time and porosity. The fastest solidification proceeds the most advantageous it is for the resulting microstructure. Porosity is measured on a 0-1 scale and is distinguished into micro- (<0.01) and macro-porosity (>0.01). In general a value lower than 0.2 is considered acceptable locally, however, overall acceptability depends also on distribution of pores. In experimenting with mold geometry it was decided to remove the bottom plate and compare results with those corresponding to the original two plate design, see Table 2. Characteristic snapshots regarding solidification time and porosity are shown in figure 4.

Table 2. Solidification simulation results (G: gravity, V: Vacuum, N: negligible)

Case	1	2	3	4	5	6	7	8	9	10	11	12	13	14	15	16
Casting type	G	G	G	G	G	G	G	G	V	V	V	V	V	V	V	V
Number of plates	2	2	2	2	1	1	1	1	2	2	2	2	1	1	1	1
Melt temperature (°C)	650	650	700	700	650	650	700	700	650	650	700	700	650	650	700	700
Mold temperature (°C)	250	400	250	400	250	400	250	400	250	400	250	400	250	400	250	400
Solidification time (sec)	236	544	268	588	224	682	251	717	234	526	268	575	221	655	251	696
Porosity	.011	.218	.012	.52	.012	.343	.011	.52	N	N	N	N	N	N	N	N

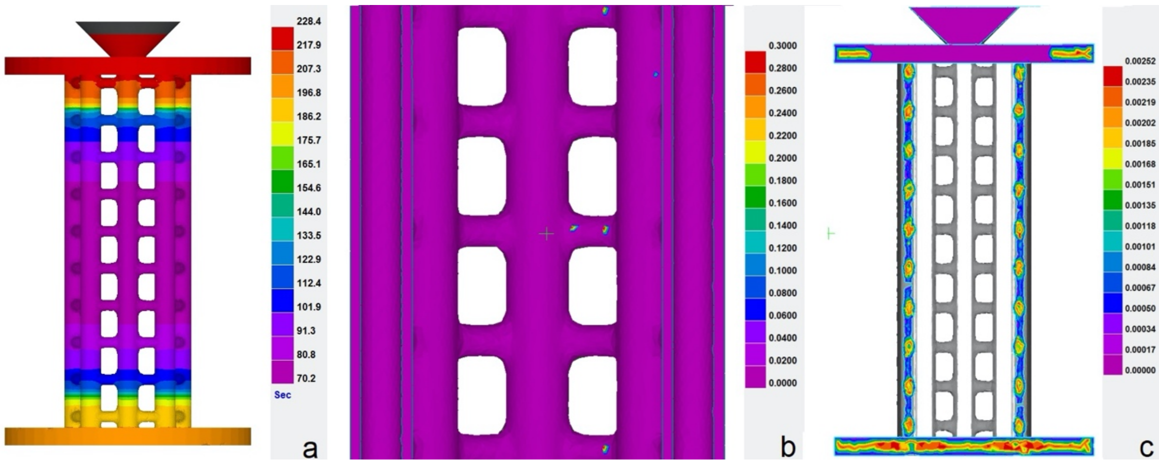

Figure 4. Calculation examples (a) solidification time (b) macro-porosity (c) micro-porosity

In summary, referring to Table 2, vacuum casting is much preferable to gravity casting, on the grounds of much reduced porosity, whereas no significant differences are observed in solidification time. Thus, Cases 1-8 in Table 2 are neglected in favour of cases 9-16. In the latter, removal of one plate is comparable to using two plates regarding solidification time for low mold temperature, compare Cases 9 and 13; thus, case 13 is preferable since it also results in material savings.

3.3. Stresses and deformation

In this part of the simulation study, the mold was defined as rigid. In the simulation program's database mechanical properties of the material (A356), including thermal expansion coefficient, are available as a function of temperature. Computation load is high, therefore only the best case of Table 2 is examined, namely case 13. Of particular interest is the distribution of residual stresses as a result of inhomogeneous cooling and contraction of the casting, hot cracking sensitivity and deformation resulting from contraction. Simulation results are shown in figure 5.

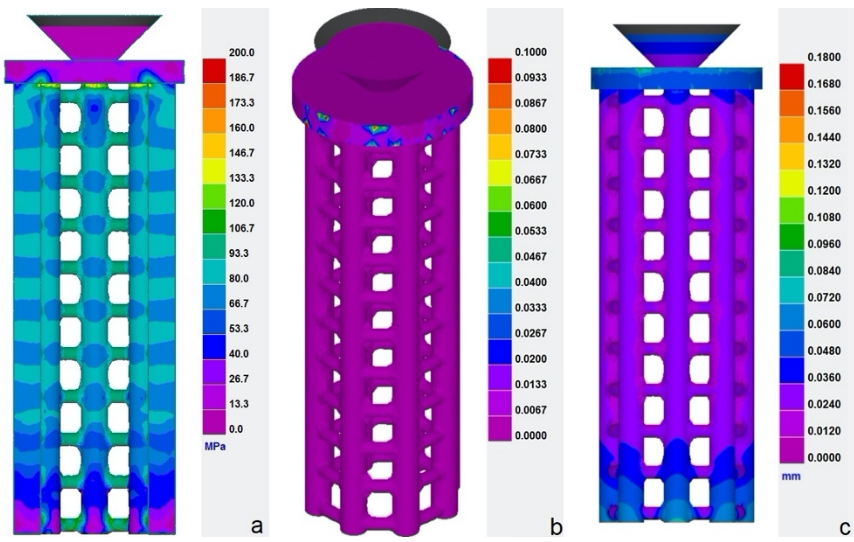

Figure 5. Stress analysis for case 13 (a) residual stresses (b) hot cracking sensitivity (c) deformation

Areas at the junction of two sections of largely different casting modulus as well as mass, notably junctions of plate and vertical rods, exhibit large differences in contraction (displacement) hence deformation is developed which is associated with the emergence of residual stresses, compare figures 5(a) and (c). This is also obvious on the finite element mesh in its initial and final state, see figure 6.

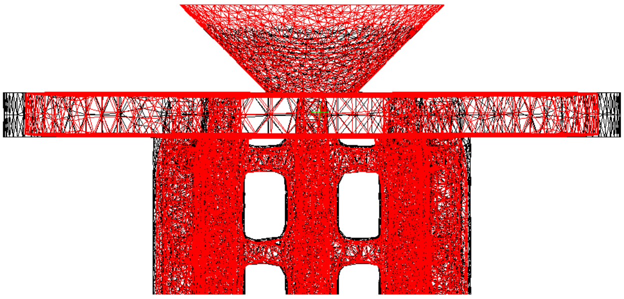

Figure 6. Initial (black, pre-contraction) and final (at room temperature, red) finite element mesh.

Hot cracking sensitivity (HCS) prediction is based on the RDG criterion [14], i.e. effectively in the pressure drop that is observed locally in solid-liquid coexistence areas due to deformation / shrinkage. This is an integral part of the casting simulation platform used. HCS index is the inverse of the maximum local deformation rate, high values corresponding to high probability of cracking. In our case the part as such is not prone to cracking, whereas some areas of the plate are mildly susceptible, see figure 5(b).

Deformation (displacement) is observed at the plate and sprue, which is unimportant, since these parts are cut off eventually. Deformation at the two ends of the spacer is deemed tolerable, see figure 5(c).

4. Investment casting prototyping

A prototype specimen was cast with the lost wax method. A wax model was initially manufactured manually by welding together wax rods of the appropriate shape and cross section, but it soon became apparent that the result was not of industrial calibre. Thus, an appropriate mold accounting of 1/16th of the original part was 3D printed using a resin and powder mix, see figure 7(c).

This mold was used in a wax casting machine at a relative pressure of 0.25 bar και temperature of 85°C in order to produce a number of identical module wax models, see figure 7(d). Sixteen of these models were then welded together by use of an electric soldering iron thereby assembling a full wax model, see figures 7(a) and 7(b).

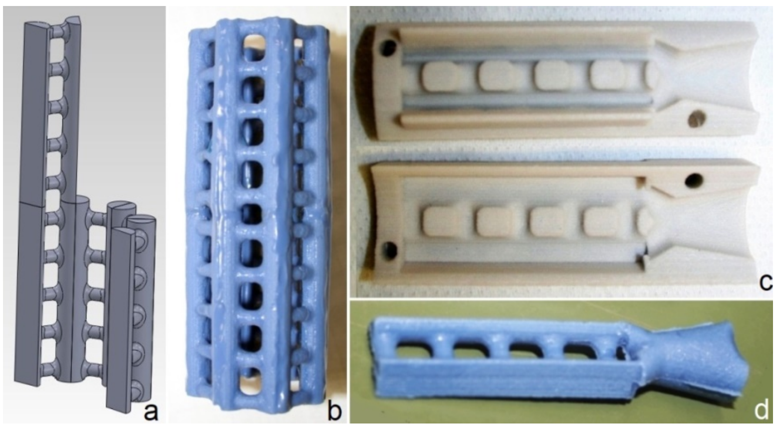

Figure 7. Wax model (a) partial assembly design (b) assembly (c) 3D printed mold (d) wax module

The alternative of using a special 3D printer to make the wax model directly, thereby avoiding wax molding, was considered expensive, because 3D printing a mold allows exploiting it indefinitely to create as many wax models as desired.

Following the investment casting process prescription, the wax model was put in a flask and plaster (Argentum Jewelry Investment by Ransom &Randolph) was poured around it. A vacuum machine was employed in order to eliminate all air bubbles trapped in the plaster while being in the flask. Upon solidification of the plaster a dewaxing oven was used in order to remove the wax model through melting it at 200^{o}C for 90 min. Then, the plaster mold was baked in a special oven for 6 hrs to 750^{o}C to increase its strength This plaster mold was employed in a vacuum casting machine, see figure 8(a), casting conditions corresponding to Case 13 of Table 2. The resulting casting was only partly satisfactory, discrepancies being mainly due to surface roughness and presence of surface defects, see figure 8(b). This was directly attributable to inadequate pressure difference between the vacuum and casting chambers of the machine due to wear and tear.

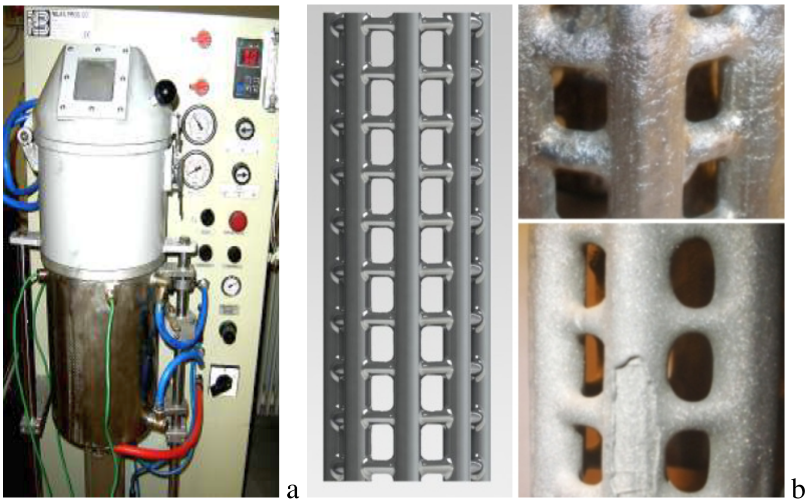

Figure 8. (a) Vacuum casting machine used (b) casting with roughness and surface defects

5. Conclusions

A case study was presented regarding design and manufacture of a mesh-like cylindrical spacers intended for structural applications under a combination of axial and mostly shear loads. As a roadmap for such engineering tasks, the following conclusions are drawn.

The most favorable shape results from static elastic loading simulation for several versions of the parametrically designed part based on a composite evaluation function involving both maximum observed stress and maximum observed deformation, compared to allowable values, as well as mass of the part.

This shape is then considered for casting, a process that can achieve considerable shape complexity at low cost. Casting simulation on a specialized platform is most valuable in studying intended feeding system as well as casting type and parameters. Filling completeness, solidification time and porosity defects are the immediate criteria on which alternatives can be judged. The best alternative is then examined in terms of residual stresses, deformation and hot cracking sensitivity. Vacuum casting proved superior to gravity casting; similarly, low compared to high mold temperature favored low solidification time. Overall adequacy of an unorthodox feeding system was also ensured.

Symmetrical shapes benefit from 3D printed molds for casting wax modules that are assembled by surface heating. Lost wax investment casting involves a number of successive stages, which are well documented, but the final quality of the part depends heavily on possible vacuum casting machine's wear especially at the interface surfaces between flask, casting and vacuum chambers.

References

[1] Helou M and Kara S Design, analysis and manufacturing of lattice structures: An overview 2018 *Int. J. Comput. Integr. Manuf.* **31** 243–61
[2] Panesar A, Abdi M, Hickman D and Ashcroft I Strategies for functionally graded lattice structures derived using topology optimisation for Additive Manufacturing 2018 *Addit. Manuf.* **19** 81–94
[3] Tsavdaridis K D, Nicolaou A, Mistry A D and Efthymiou E Topology optimisation of lattice telecommunication tower and performance-based design considering wind and ice loads 2020 *Structures* **27** 2379–99
[4] Daynes S, Feih S, Lu W F and Wei J Design concepts for generating optimised lattice structures aligned with strain trajectories 2019 *Comput. Methods Appl. Mech. Eng.* **354** 689–705
[5] Daynes S, Feih S, Lu W F and Wei J Optimisation of functionally graded lattice structures using isostatic lines 2017 *Mater. Des.* **127** 215–23
[6] Maliaris G and Sarafis E Mechanical behavior of 3D printed stochastic lattice structures 2017 *Solid State Phenom.* **258 SSP** 225–8
[7] Huang Y, Xue Y, Wang X and Han F Effect of cross sectional shape of struts on the mechanical properties of aluminum based pyramidal lattice structures 2017 *Mater. Lett.* **202** 55–8
[8] Xue Y, Wang X, Wang W, Zhong X and Han F Compressive property of Al-based auxetic lattice structures fabricated by 3-D printing combined with investment casting 2018 *Mater. Sci. Eng. A* **722** 255–62
[9] Pagratis N, Karagiannis N, Vosniakos G C, Pantelis D and Benardos P A holistic approach to the exploitation of simulation in solid investment casting 2007 *Proc. Inst. Mech. Eng. Part B J. Eng. Manuf.* **221** 967–79
[10] Khan M A A and Sheikh A K Simulation tools in enhancing metal casting productivity and quality: A review 2016 *Proc. Inst. Mech. Eng. Part B J. Eng. Manuf.* **230** 1799–817
[11] Vosniakos G-C, Michael S and Vasileiou A Digital Manufacturing Process Chain for One-Off Replacement Parts: A Precision Casting Case Study 2017 *J. Manuf. Mater. Process.* **1** 17
[12] Krimpenis A, Benardos P G, Vosniakos G C and Koukouvitaki A Simulation-based selection of optimum pressure die-casting process parameters using neural nets and genetic algorithms 2006 *Int. J. Adv. Manuf. Technol.* **27** 509–17
[13] Vasileiou A N, Vosniakos G C and Pantelis D I Determination of local heat transfer coefficients in precision castings by genetic optimisation aided by numerical simulation 2015 *Proc. Inst. Mech. Eng. Part C J. Mech. Eng. Sci.* **229** 735–50
[14] Drezet J M and Rappaz M Prediction of Hot Tears in DC-Cast Aluminum Billets 2013 *Essent. Readings Light Met.* **3** 912–8